Hindawi
Geofluids
Volume 2023, Article ID 2132017, 15 pages
https://doi.org/10.1155/2023/2132017

Research Article

Conventional Mercury Penetration and Constant Velocity Mercury Penetration Experiments Are Used to Quantitatively Characterize the Difference in Micropore Structure in Low Permeability Reservoirs and Its Influence on Movable Fluid Saturation

Kaitao Yuan,[1] Yan Li,[1] Tiaotiao Shi,[2] Husheng Huang,[1] Yanfei Li,[1] and Minglei He[1]

[1]*Dingbian Oil Production Plant of Yanchang Oil Field Co., Ltd., Yulin 718600, China*
[2]*Research Institute of Shaanxi Yanchang Petroleum (Group) Co., Ltd., Xi'an 710075, China*

Correspondence should be addressed to Yan Li; ycoilfield_yanli@163.com

Received 2 June 2022; Revised 9 September 2022; Accepted 10 October 2022; Published 19 April 2023

Academic Editor: Dengke Liu

There are many research methods and experimental means for quantitative and semiquantitative evaluation of low permeability reservoirs. Generally, people do not use a single means to study them but use a variety of experimental means to verify and complement each other. Conventional mercury penetration and constant velocity mercury penetration are two important experimental methods for the quantitative evaluation of tight reservoirs. The micro characteristic parameters of reservoirs obtained by them are quite different, which bring some difficulties to people's research. This paper first analyzes the reasons for the differences between the two from the aspects of experimental theory and model, experimental conditions, and experimental process. Taking C 6 and C 7 reservoirs in Ordos Basin as an example, a total of 13 representative pairs of samples were selected to analyze the difference in capillary pressure curve shape and pore throat distribution characteristics between the two experiments and to clarify the reasons for the difference in microscopic pore characteristic parameters measured by the two experiments. Finally, the correlation between the microscopic pore characteristic parameters and the movable fluid saturation parameters is analyzed. The results show that the theoretical model of conventional mercury penetration experiment is a capillary tube bundle model with different radii. The maximum injection pressure of experimental mercury is high and the experimental speed is fast. The theoretical model of constant velocity mercury penetration experiment is the pore and throat capillary model with different radii. The maximum injection pressure is low, the experimental speed is very slow, and the process is quasistatic. The parameters such as displacement pressure, total mercury saturation, and separation coefficient obtained by the latter are smaller than those measured by the former; however, the maximum throat radius, average throat radius, and other parameters obtained by the latter are larger than those measured by the former. According to the correlation chart drawn, it can be concluded that the correlation between the microscopic pore throat characteristic parameters and the movable fluid saturation in the constant velocity mercury penetration experiment is better than that in the conventional mercury penetration experiment. The influencing factors mainly include permeability, porosity, displacement pressure, maximum pore throat radius, and sorting coefficient. The maximum mercury injection saturation has little correlation.

1. Introduction

Petroleum geologists believe that the study of micropore structure is still one of the hotspots and difficulties in the research of the tight reservoirs. The pore throats are small and have strong microheterogeneity. Therefore, the micropore structure composed of them needs to be complemented by a variety of experimental methods and more advanced experimental means

for quantitative research, so as to obtain relatively satisfactory research results [1–7]. There are two experimental methods to quantitatively study the micropore structure, including the direct method and the indirect method. Among them, conventional mercury penetration and constant velocity mercury penetration experiments are the two most important experiments for quantitatively researching the features of tight reservoirs [8–13]. Researchers must use these two experimental methods as long as they conduct fine and microscopic reservoir research. However, the measured parameters of these two experimental methods are quite different, which brings some confusion to data users. This paper selects 13 pairs of representative samples from C 6 and C 7 formations and analyzes the reasons for the differences in the same kind of parameters measured by these two experiments from the aspects of experimental theory and model, experimental conditions, and experimental process [14–17]. It solves the problem that there are differences between the two when researchers use experimental parameters to evaluate reservoirs. It has practical significance to solve the problems encountered in practical experiments.

2. Geological Background

Based on the experimental data and photos, the typical characteristics of C 6 and C 7 formations are briefly analyzed and introduced. The lithology of C 6 formation is mainly fine-grained arkose and lithic arkose, most of which are gray-black and gray (Figure 1). The clastic composition is mainly feldspar, with an average value of 57.7%. The second is quartz, with an average value of 22.25%. There is also a small amount of rock debris, which is 11.55%. The rock debris type is mainly metamorphic rock, accounting for 4.63%. The quantity of interstitial materials is 8.00%, and the main interstitial materials are chlorite, ferricalcite, hydromica, siliceous, and feldspathic (Figures 2(a)–2(c)). The main particle size is between 0.12 and 0.40mm. It has a good particle sorting. The second edge dominates the roundness of particles, mainly pore film cementation. Porosity is 10.38% and permeability is 0.60×10^{-3} μm^2. The rock type of C 7 reservoir is mainly very fine-grained arkose, and the colors include grayish black, gray, and grayish white (Figures 1 and 2(d)). The clastic composition is mainly feldspar, with an average value of 48.8%. The second is quartz, with an average of 24%. There is also a small amount of rock debris, which is 7.6%. The rock debris type is mainly metamorphic rock, with 7.4%. The quantity of interstitial materials is 13.1%. The main interstitial materials are calcite, iron calcite, chlorite, feldspathic, illite and silica, and a small amount of hydromica (Figure 2(f)). The main particle size is between 0.10 and 0.24 mm. The particle sorting is in the good medium level. The roundness of particles is mainly subedge subcircle, mainly porous cementation and film pore cementation (Figure 2(e)). The porosity is 10.1%, and the permeability is 0.46×10^{-3} μm^2.

3. Experiment

The instrument selected in this conventional mercury penetration experiment is AutoPore IV 9500 (instrument number: 20113083). The model of constant-speed mercury penetration experimental instrument is ASPE-730 (instrument number: 14114383). The test basis is GB/T29171-2012. The reasons for the differences in the experimental results will be analyzed from the aspects of experimental theory and model, experimental conditions, and experimental process.

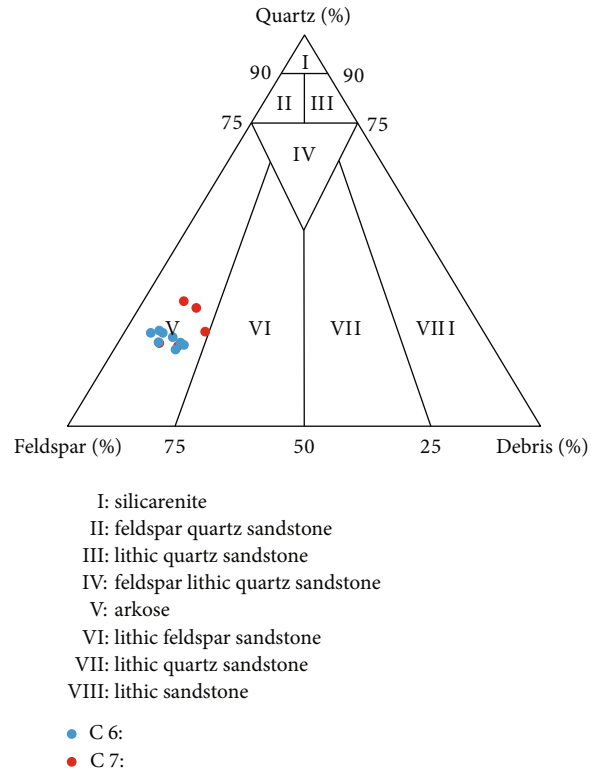

Figure 1: Rock type classification of C 6 and C 7 layers.

3.1. Differences in Theory and Model between Conventional Mercury Penetration and Constant-Speed Mercury Penetration Experiments

3.1.1. Experimental Principle. The theoretical principles of the two experiments are basically the same. That is, the mercury penetration agent is a nonwetting phase to most cores. If mercury is pressed, when the applied pressure can exceed the capillary pressure, mercury can smoothly get into the throats and the pores they control. According to the corresponding mercury saturation increment under a certain pressure, the capillary pressure curve can be drawn.

Under normal temperature and pressure, σ is 0.48N/m, and θ is 140°; then, the simplified formula can be obtained.

$$P_c = \frac{0.735}{r_c}. \quad (1)$$

According to the capillary radius and mercury saturation increment, the pore throat distribution histogram can be obtained.

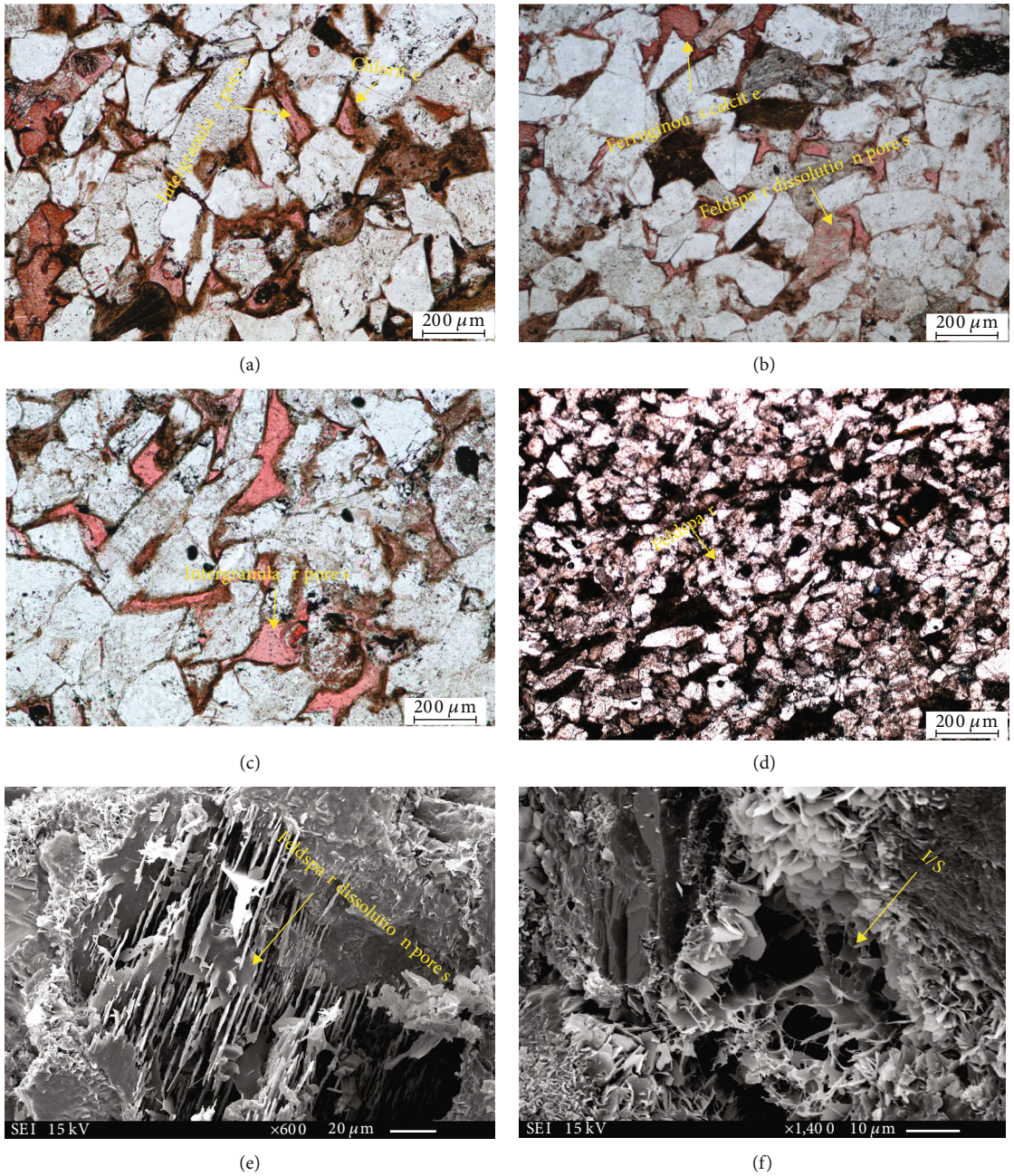

Figure 2: Typical photos of C 6 and C 7 formations. (a) Intergranular pore, chlorite, well X 28, C 6. (b) Intergranular pore, ferrocalcite, well X 39, C 6. (c) Chlorite, intergranular pore, well X 13, C 6. (d) Very fine-grained arkose, well D 6266, C 7. (e) Feldspar dissolution, well D 1978, C 7. (f) Yimeng mixed layer, well D 6547, C 7.

3.1.2. Experimental Theoretical Model. The theoretical models of the two experimental hypotheses are different [17]. The theoretical model of the conventional mercury penetration experiment is assumed to be bundle models with various radii (Figure 3(a)). The theoretical model of the constant velocity mercury penetration experiment is assumed to be pores and throats with various radii (Figure 3(b)). The theoretical model hypothesized in the former experiment could not distinguish between pores and throats, while the theoretical model hypothesized in the latter experiment can distinguish between pores and throats. Therefore, the latter experiment assumes that the theoretical model is closer to the real situation of low permeability and low porosity reservoirs.

3.2. Differences of Experimental Conditions. These two experiments were carried out at room temperature, but the maximum pressure reached was different. In the conventional mercury penetration experiment, the maximum injection pressure can reach 206 MPa; but of the constant-speed mercury penetration experiment, the pressure is about 6.89 MPa (1000 psi). According to the formula, the minimum throat radius measured in the former experiment can reach 0.0035 μm. The minimum pore throat radius

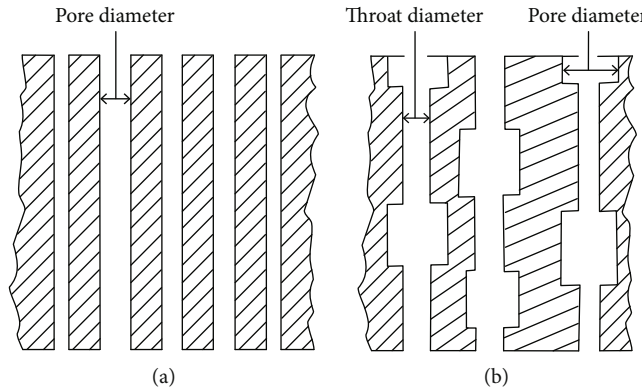

Figure 3: Experimental model diagram (modified by Puli Chen). (a) Conventional mercury penetration model. (b) Constant-speed mercury penetration model.

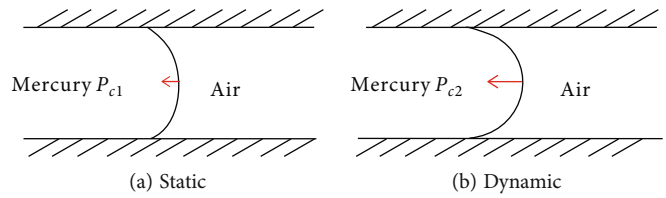

Figure 4: Schematic diagram of dynamic and static capillary pressure.

measured in the latter experiment is as high as 0.107 μm. Therefore, limited by the experimental pressure, the range of pore throat radius measured in the former experiment is far greater than that tested in the latter experiment.

3.3. Differences in Experimental Process. The experimental process of these two mercury injection methods is basically the same. The difference is mainly reflected in the experimental speed. The conventional mercury penetration experiment is fast, and the whole experiment can be completed within one to two hours. The constant-speed mercury penetration experiment is conducted at an extremely low fixed speed (usually 0.00005 ml/min), during which the mercury injection process remains quasistatic. The whole experimental process takes two to three days, and if the permeability is lower, it will take longer. Obviously, the experimental speed has a fundamental impact on the experimental results.

First, in the conventional mercury penetration experiment, due to the fast injection rate and the dynamic equilibrium of the whole system, the meniscus will become larger, resulting in the measured pore throat radius being larger than the actual value (Figure 4(b)). In the latter experiment, the mercury feeding speed was slow enough, and the whole system was in quasistatic equilibrium, and the test result approached the true value (Figure 4(a)).

Second, in constant-speed mercury penetration experiment, because the mercury feeding speed is fast, the pressure holding and pressure releasing processes cannot be separated, so only the capillary pressure curve of the whole pore throat can be acquired. The whole experimental process of the latter experiment remains quasistatic. When mercury enters each throat with a small radius, it will hold the pressure, and at this time, the pressure rises. When mercury comes out of the throat and enters each pore with a small radius, the pressure is released and the corresponding pressure is reduced. During a series of pressure rise and drop experiments, the capillary pressure curve of the throat and pore can be acquired, respectively, so the pore and throat can be distinguished.

4. Results and Discussions

The above is to research the causes for the differences between the two experiments from the aspects of experimental theory and experimental model, experimental conditions, and experimental process. In this paper, 13 pairs of samples are selected for example analysis, including 8 samples in C 6 reservoir and 5 samples in C 7 reservoir. Each pair of samples belongs to the same depth of the same well, which is highly comparable. The following examples are used for analysis and verification. In the research process, the capillary pressure curve shape and micropore throat characteristic parameters were compared one by one to analyze their comparability and the reasons for differences. The research conclusions have definite guiding significance and reference significance for technicians to analyze the microscopic characteristics of reservoirs using the two kinds of experimental data.

4.1. Comparison of Distribution Characteristics of Pore Radius, Throat Radius, and Pore Throat Ratio. The main pore radius distribution of the C 6 formation is between 110 and 180 μm, the radius distribution of the main throat is between 0.25 and 3.25 μm, and the pore throat ratio is mainly between 80 and 340 (Figures 5(a)–5(c)). The main pore radius distribution of C 7 reservoir is between 100 and 160 μm, and the radius distribution of the main throat is between 0 and 0.5 μm, and the pore throat ratio is mainly between 200 and 800 (Figures 6(a)–6(c)). Because C 6

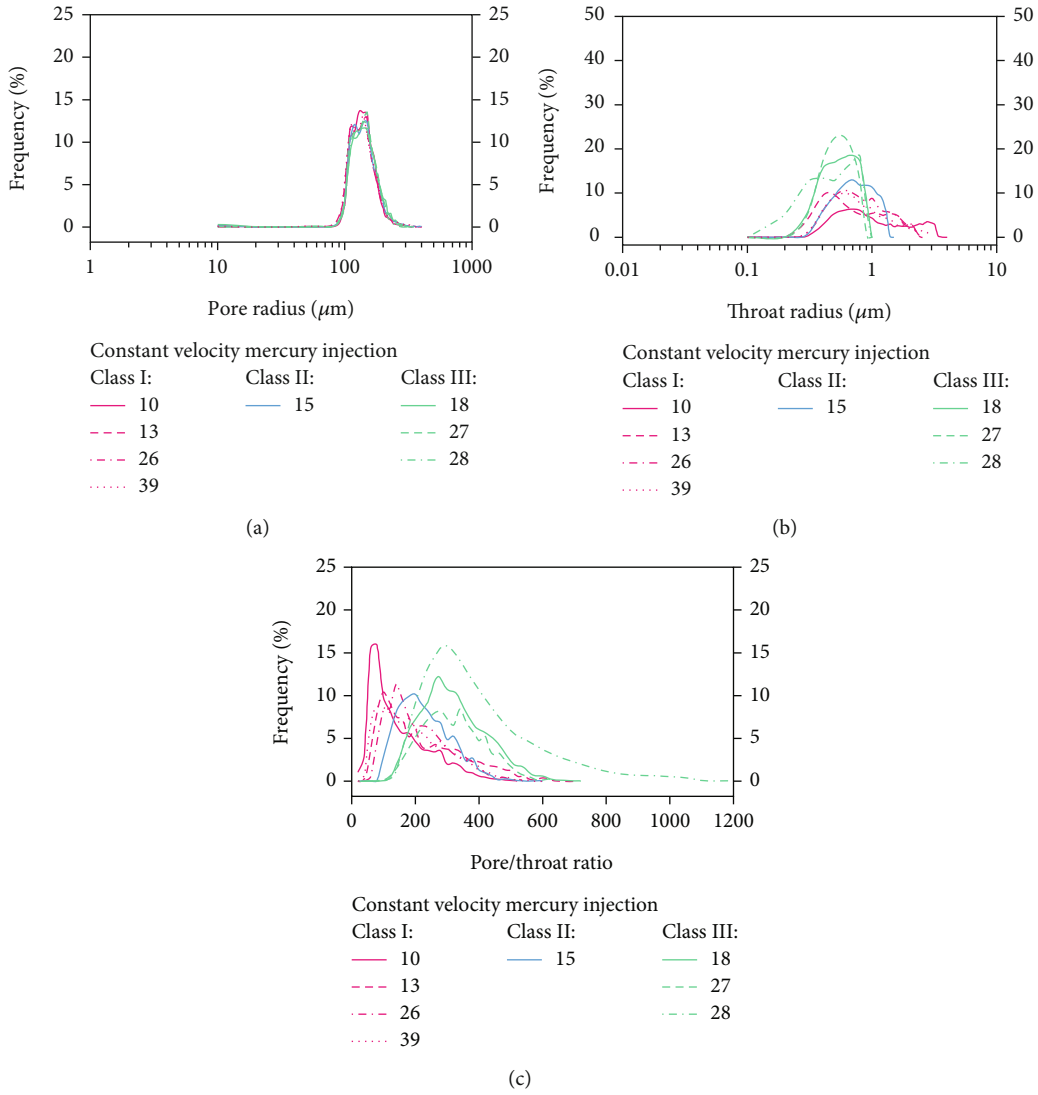

Figure 5: Distribution frequency curve of pore radius, throat radius, and pore throat ratio in constant velocity mercury penetration test of C 6 reservoir.

reservoir has better physical properties, the distribution limit of throat radius and pore radius is wider, while C 7 reservoir has worse physical properties, larger pore throat ratio, and stronger microheterogeneity.

4.2. Comparison of Capillary Pressure Curve Shape and Pore Throat Distribution

4.2.1. Comparison of Curve Shapes. There is a great difference between the two experimental capillary pressure curves (Figures 7 and 8). The conventional mercury penetration experiment consists of one capillary pressure curve, while the constant-speed mercury penetration experiment can obtain three. According to the curves drawn from the test data of the two experiments, the pore structures of C 6 and C 7 can be divided into four types, of which C 6 reservoir is of class I, II, and III micropore structures, and C 7 reservoir is of class III and IV micropore structures. It can be seen from the curve shape that pores play a certain leading role in the early stage of development. With the increase of pressure, throats begin to play a major role (Figures 8(a) and 8(b)) [18]. By analyzing the reasons for the differences in feature parameters, we can better guide the research work.

4.2.2. The Comparison of Pore Throat Distribution Characteristics. From the above 13 samples, select representative samples to analyze the two experimental results.

Three blocks representing class I (no. 13), class II (no. 15), and class III (no. 27) of microporous phenology are selected for C 6 layer, and two blocks representing class III (no. 23) and class IV (no. 47) of microporous phenology are selected for C 7 layer.

Among the three types of curves of conventional mercury penetration in C 6 reservoir (Figure 9), the pore throat distribution curve has two peaks, and the corresponding cumulative mercury penetration curve rises rapidly. The first peaks of class I (Figure 9(a)), class II (Figure 9(b)), and class III (Figure 9(c)) are in turn nano-micropore throats and micropore throats, nano-micropore throats, and nano-micropore and micro-nanopore throats. Therefore, the

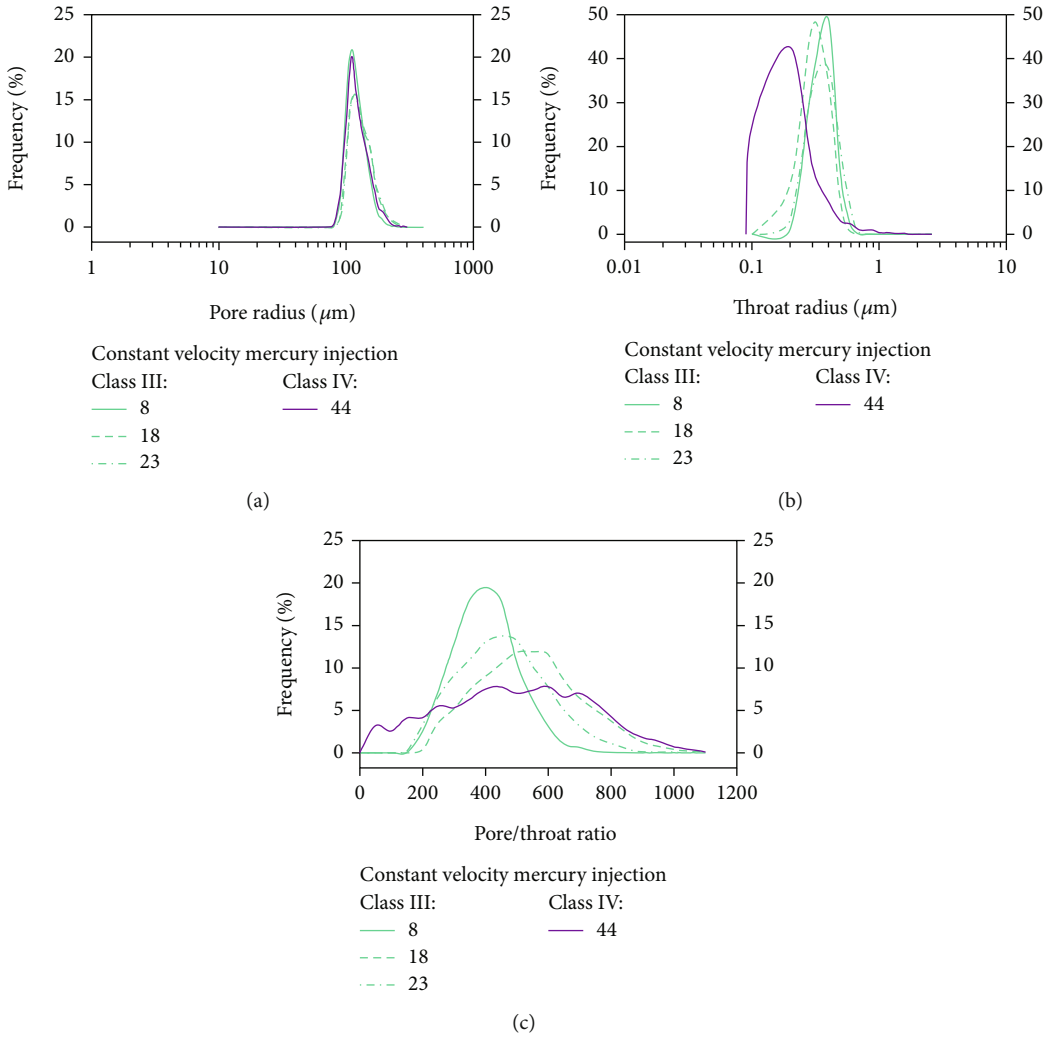

Figure 6: Distribution frequency curve of pore radius, throat radius, and pore throat ratio in constant velocity mercury penetration test of C 7 reservoir.

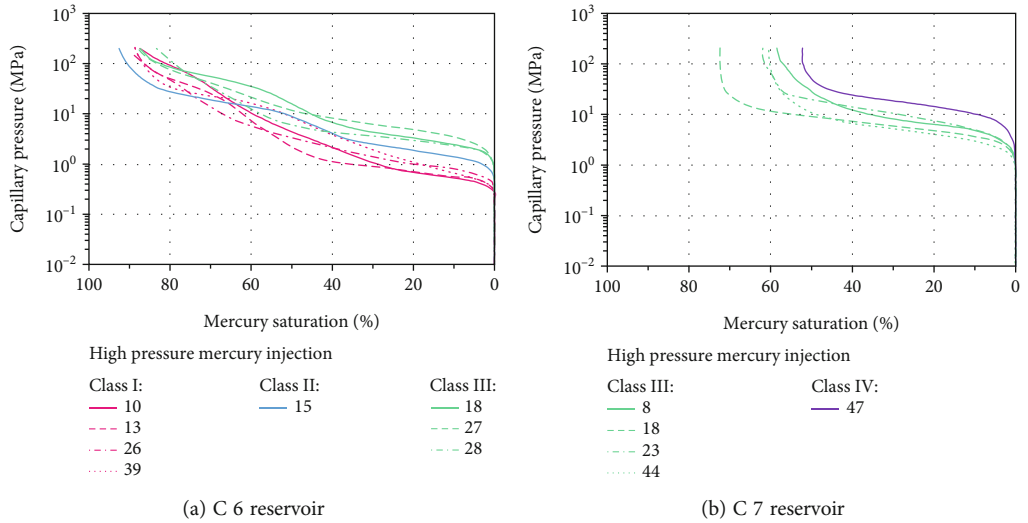

Figure 7: The capillary pressure curve of high-pressure mercury penetration experiment.

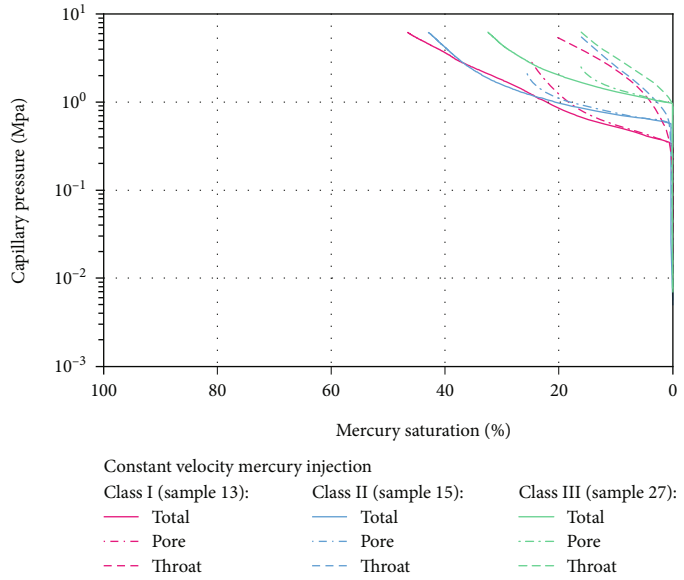

(a) C 6 reservoir

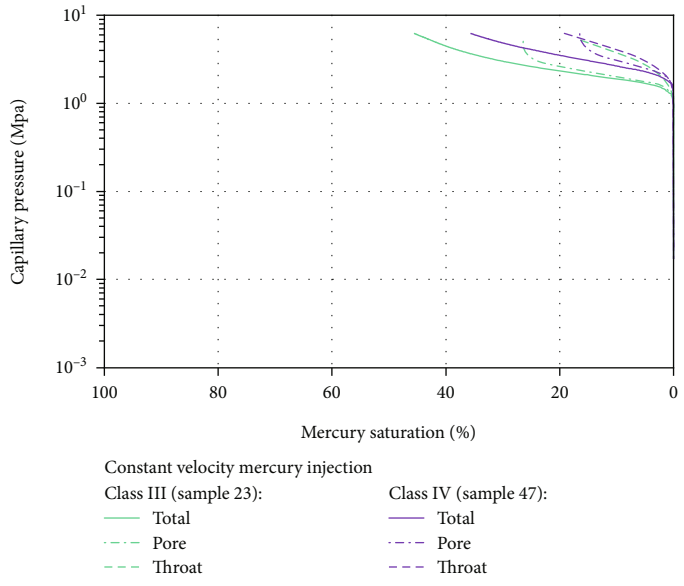

(b) C 7 reservoir

Figure 8: The capillary pressure curve of constant-speed mercury penetration experiment.

corresponding radius gradually decreases. The second peak pore throat radius of the third class of pore throat is smaller, both of which are nanopore throat and micro-nanopore throat. The pore and throat distribution curve of the latter experiment has one peak, which belongs to nano-micropore throats.

The pore throat distribution curve of C 7 reservoir is tending to contrast with that of C 6 layers (Figure 10). The pore throat distribution curve of the former experiment has only one peak, and all are micro-nanopore throats, and the corresponding cumulative mercury injection curve rises at a high speed. In the latter experiment, both the pore distribution curve and the throat distribution curve have one peak, belonging to nano-micropore throats, and the peak value of the pore distribution curve is larger than that of the throat.

4.3. The Comparison of Characteristic Parameters of Micropore Structure. Select the two kinds of experimental micro characteristic parameters that can reflect the reservoir to compare one by one, and analyze the reasons for their differences [19–22].

4.3.1. Displacement Pressure. In Table 1, samples X10 to X 39 belong to C 6 reservoir, and samples D8 to D 47 belong to C 7 reservoir. Obviously, the displacement pressure of constant-speed mercury penetration experiment is lower than that of conventional mercury penetration experiment.

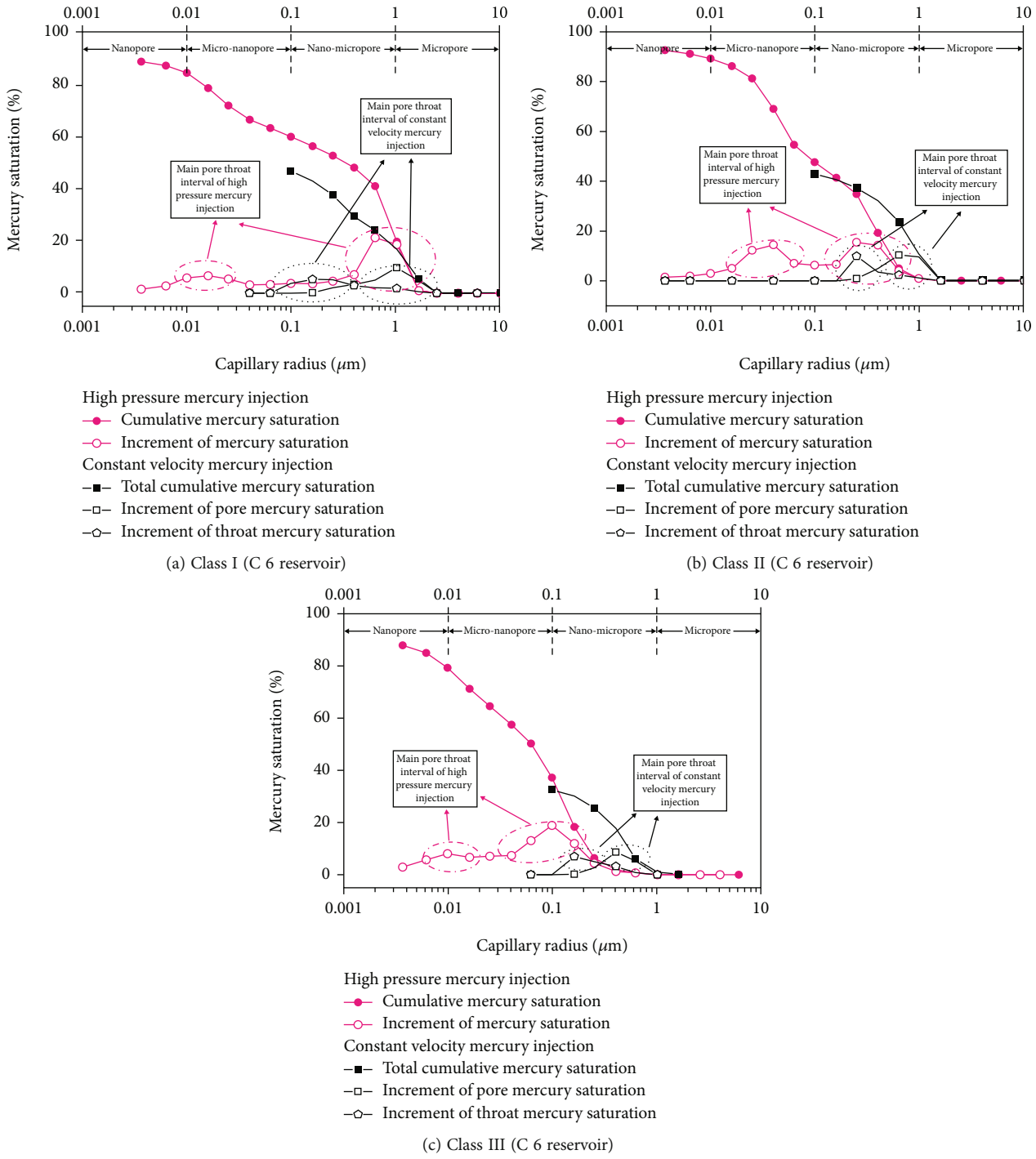

Figure 9: Superposition diagram of pore throat distribution and cumulative mercury saturation curve of C 6 reservoir.

This is because the experimental speed of the former experiment is slow enough. During the experiment, mercury displacement first enters the largest pore throat. There is enough time to find and enter from the largest pore throat, and the measured minimum displacement pressure is low. The experimental speed of the latter is faster, and the displacement phase lacks sufficient time to find the largest pore throat and enter, and the experimental pressure rises rapidly in this process, and the lowest displacement pressure measured is relatively high.

4.3.2. Maximum Mercury Saturation. The maximum mercury saturation of the conventional mercury penetration experiment is greater than the total mercury saturation acquired by the constant-speed mercury penetration experiment (Table 1). Analyzing the experimental conditions, the

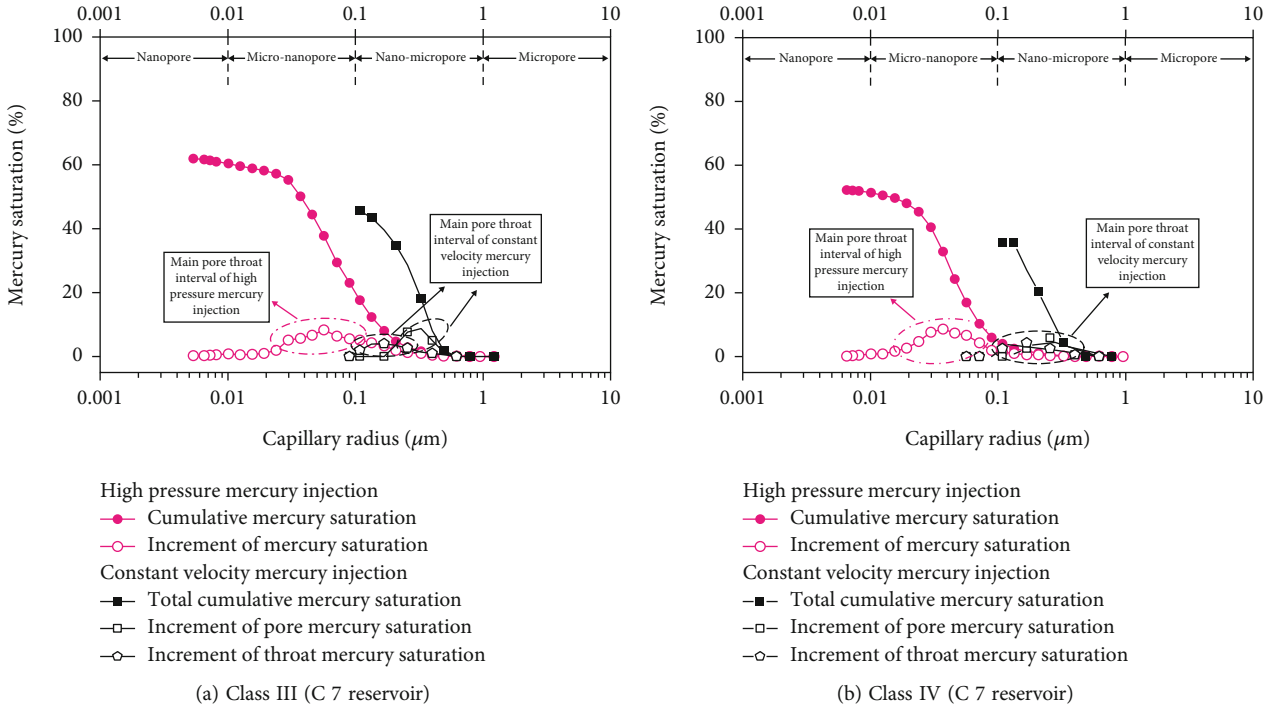

(a) Class III (C 7 reservoir)

(b) Class IV (C 7 reservoir)

Figure 10: Superposition diagram of pore throat distribution and cumulative mercury saturation curve of C 7 reservoir.

Table 1: Typical parameters of micropore structure (displacement pressure and mercury saturation).

Sample number	Permeability ($\times 10^{-3}$ μm^2)	Porosity (%)	Displacement pressure (MPa)			Maximum mercury saturation		Mercury saturation at 6.89 MPa	①-②	②-③
			①	②	①-②	①	②	③		
X10	1.09	12.1	0.30	0.20	0.10	87.4	59.5	41.5	27.9	18.0
X13	1.22	12.0	0.40	0.30	0.10	88.6	46.6	42.5	42.0	4.1
X15	0.32	9.3	0.70	0.60	0.20	92.6	42.9	40.6	49.6	2.3
X18	0.17	9.0	1.10	0.90	0.30	87.4	53.5	41.5	33.9	11.9
X26	1.01	11.2	0.50	0.40	0.00	90.0	49.1	44.8	41.0	4.3
X27	0.19	9.0	1.20	1.00	0.20	87.9	32.5	31.2	55.4	1.3
X28	0.21	9.0	1.20	0.80	0.30	83.3	52.6	44.1	30.6	8.6
X39	0.69	11.5	0.30	0.30	0.00	88.6	46.6	42.4	42.1	4.1
D8	0.04	7.7	1.83	1.23	0.61	58.5	33.2	23.2	25.3	10.0
D18	0.10	10.9	1.83	1.47	0.36	72.4	42.7	36.6	29.7	6.1
D23	0.06	11.9	1.83	1.05	0.78	61.9	45.6	17.6	16.3	28.0
D44	0.19	8.3	1.49	0.43	1.06	60.3	47.0	40.8	13.3	6.2
D47	0.01	4.7	2.86	1.47	1.39	52.2	35.7	11.0	16.5	24.7

Notes: ①, conventional mercury penetration; ②, constant velocity mercury penetration; ③, mercury saturation at 6.89 MPa.

maximum injection pressure of the former experiment is 206 MPa, which is much higher than that of the latter experiment, which is 6.89 MPa. The higher the pressure, the more mercury will enter into the pore throat. Read the total mercury saturation when the experimental pressure of the former experiment is 6.89 MPa, and compare it with the total mercury saturation of the latter experiment. At this time, the maximum injection pressures of the two are basically the same. However, the total mercury saturation of the latter experiment is less than that of the former experiment at a pressure of 6.89 MPa (Table 1). This has a very important relationship with the experimental speed of the two in the experimental process. Therefore, the injection speed of the latter is low. Therefore, in the process of displacement, uniform displacement should be realized as much as possible to avoid the formation of high permeability channels, and the displacement area is increased. Nonwetting phase mercury can enter more pores.

Table 2: Typical parameters of micropore structure.

Layer	Sample number	Maximum throat radius (μm)		Mean throat radius (μm)		Sorting coefficient		②-①		
		①	②	①	②	①	②	Maximum throat radius (μm)	Mean throat radius (μm)	Sorting coefficient
C 6	X10	2.54	3.48	0.17	1.22	2.91	0.91	0.94	1.05	-2.00
	X13	1.69	2.24	0.32	0.72	2.70	0.54	0.55	0.40	-2.16
	X15	1.00	1.30	0.08	0.59	2.03	0.26	0.30	0.51	-1.77
	X18	0.64	0.85	0.05	0.46	2.45	0.17	0.21	0.41	-2.28
	X26	1.60	1.78	0.22	0.71	2.40	0.38	0.18	0.49	-2.02
	X27	0.63	0.76	0.06	0.37	2.22	0.14	0.13	0.31	-2.08
	X28	0.63	0.87	0.12	0.41	2.54	0.20	0.24	0.30	-2.34
	X39	2.51	2.84	0.08	0.90	2.51	0.62	0.32	0.81	-1.89
C 7	D8	0.40	0.60	0.09	0.39	1.33	0.19	0.20	0.29	-1.14
	D18	0.40	0.50	0.12	0.35	0.85	0.22	0.10	0.23	-0.63
	D23	0.40	0.70	0.09	0.40	1.15	0.24	0.30	0.32	-0.91
	D44	0.49	1.70	0.15	0.41	1.09	0.51	1.21	0.27	-0.59

Notes: ①, conventional mercury penetration; ②, constant velocity mercury penetration.

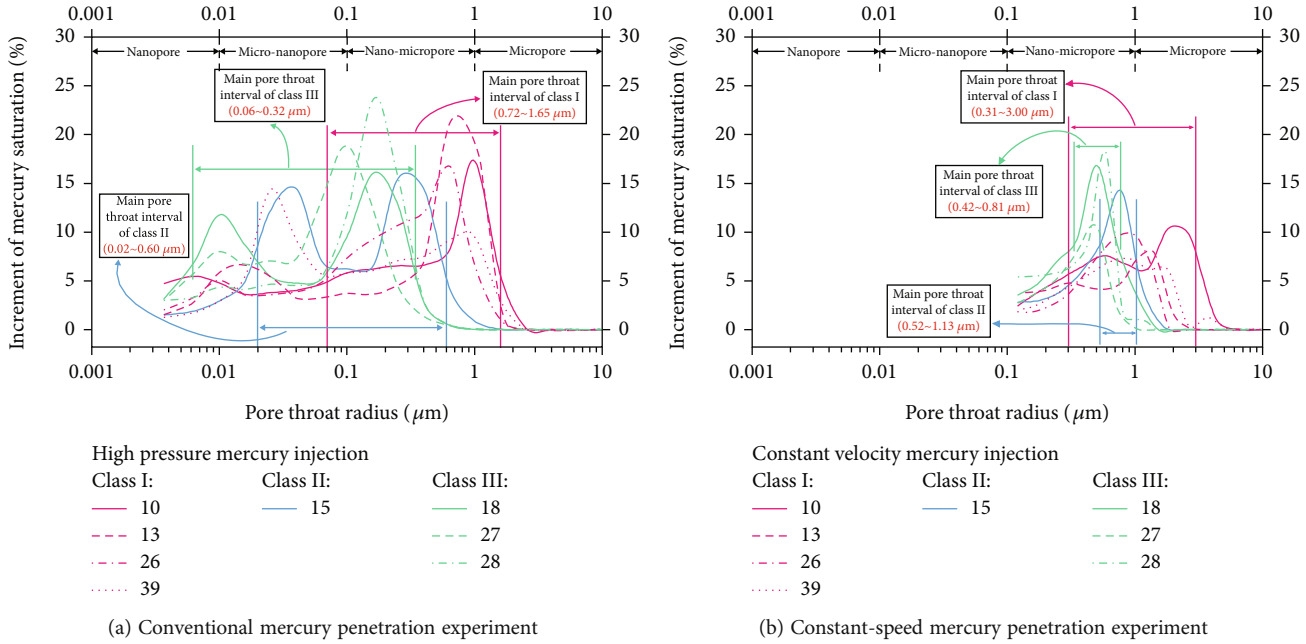

(a) Conventional mercury penetration experiment

(b) Constant-speed mercury penetration experiment

Figure 11: The frequency distribution of pore throat radius of C 6 reservoir.

4.3.3. Throat Radius. The maximum throat radius and the average throat radius measured in the constant velocity mercury penetration experiment are larger than those acquired in the conventional mercury penetration experiment (Table 2).

According to the class I, II, and III curves of the conventional mercury penetration experiment of C 6 reservoir, the radius of the main throat in turn is 0.72~1.65 μm, 0.02~0.60 μm, and 0.06~0.32 μm; the radius of the main throat of classes I, II, and III in turn is 0.31~3.00 μm, 0.52~1.13 μm, and 0.42~0.81 μm, which decreases in turn, and the main throat radius of the latter experiment is larger than that of the former experiment (Figures 11(a) and 11(b)). The curve of C 7 reservoir also shows the same law, except that the radius of the major throat of C 7 reservoir is smaller (Figures 12(a) and 12(b)).

4.3.4. Sorting Coefficient. The maximum throat radius and the average throat radius measured in the constant-speed mercury penetration experiment are larger than those measured in the conventional mercury penetration experiment, and the minimum throat radius measured by the two is significantly different (the former experiment is 0.0035 μm, and the latter experiment was 0.107 μm). Comprehensively, the

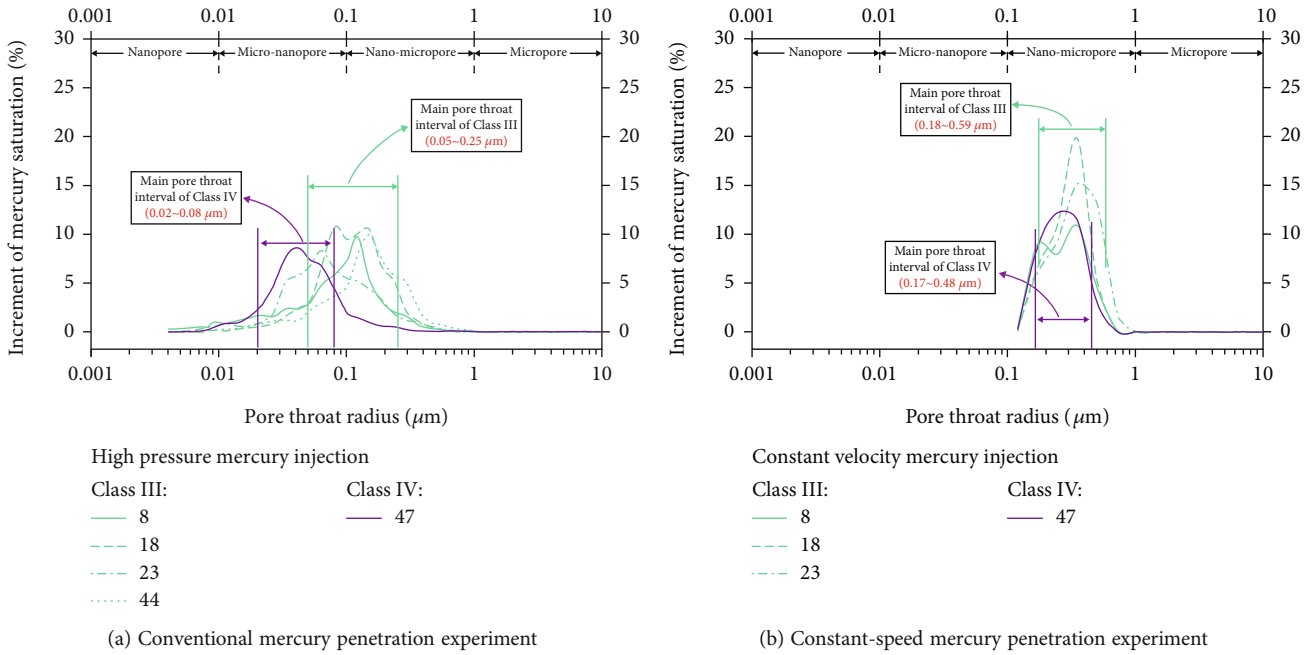

(a) Conventional mercury penetration experiment

(b) Constant-speed mercury penetration experiment

Figure 12: The frequency distribution of pore throat radius of C 7 reservoir.

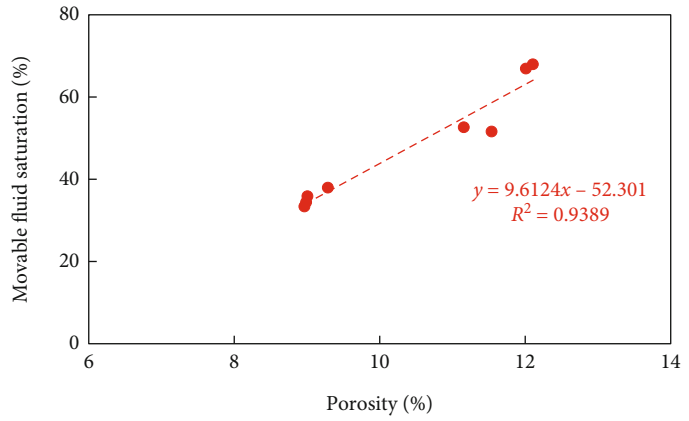

Figure 13: Relationship between porosity and movable fluid saturation.

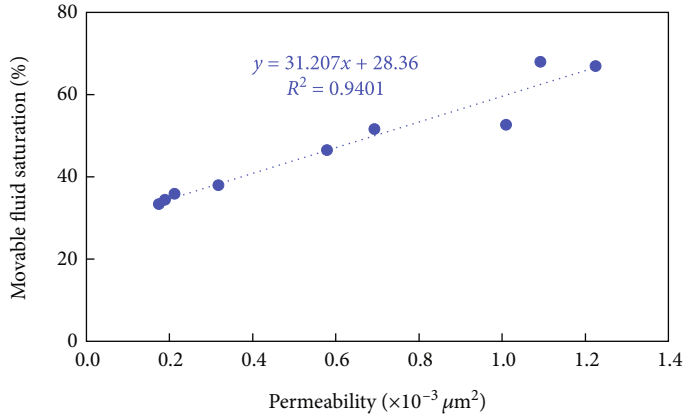

Figure 14: Relationship between permeability and movable fluid saturation.

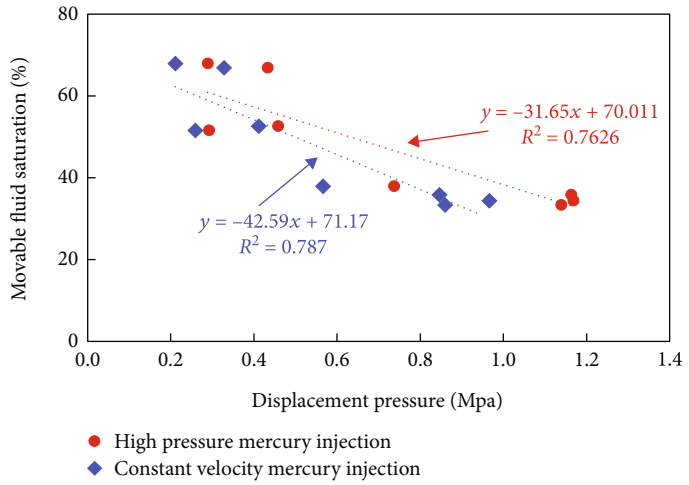

Figure 15: Relationship between displacement pressure and movable fluid saturation.

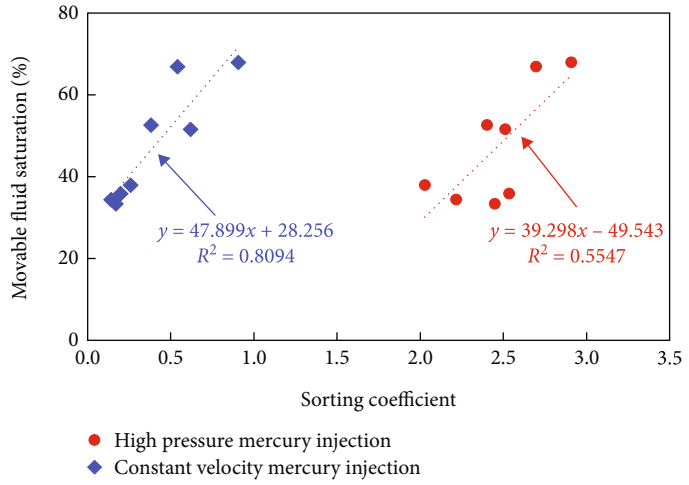

Figure 16: Relationship between sorting coefficient and movable fluid saturation.

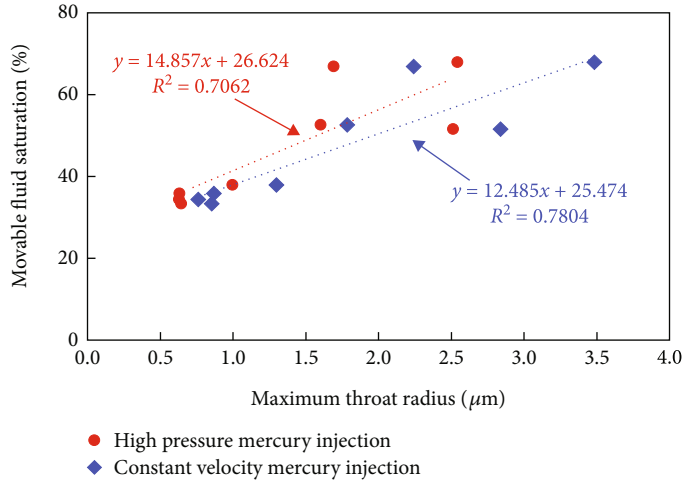

Figure 17: Relationship between maximum throat radius and movable fluid saturation.

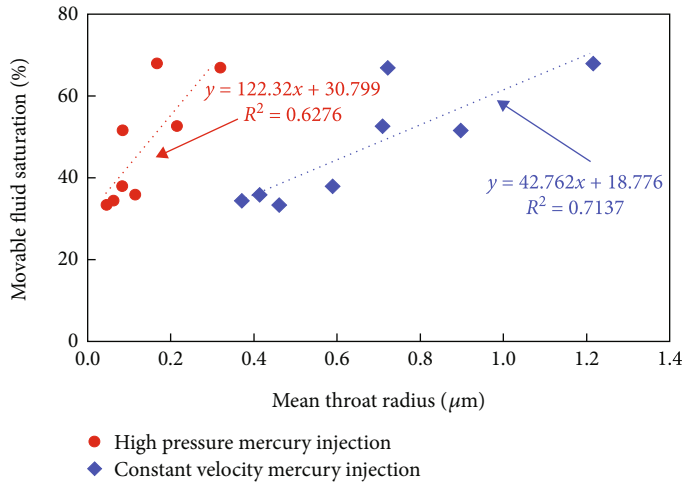

Figure 18: Relationship between mean throat radius and movable fluid saturation.

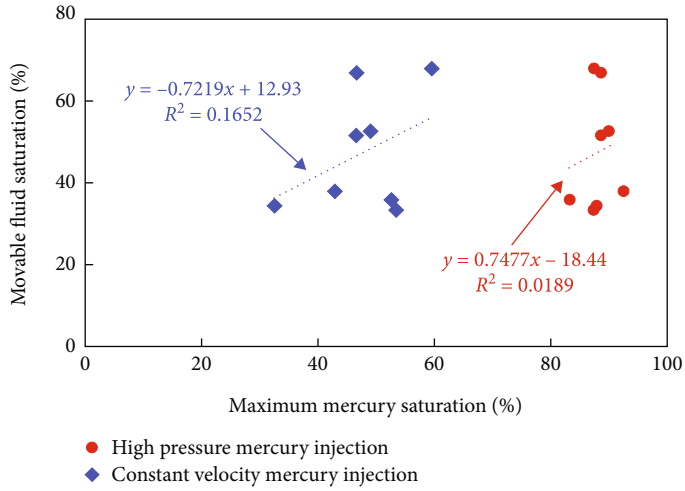

Figure 19: Relationship between maximum mercury saturation and movable fluid saturation.

throat radius sorting coefficient of the former experiment is smaller than that of the latter experiment (Table 2).

4.4. Relationship between Characteristic Parameters of Micropore Structure and Movable Fluid Saturation. Previous studies have shown that the micropore structure not only affects the physical properties but also affects the distribution of movable fluid in the pore throat.

4.4.1. Relationship with Physical Properties. The correlation between the saturation of the movable fluid and the permeability is good, but the correlation with the porosity is slightly poor, which indicates that the movable fluid of the reservoir is controlled by the percolation capacity of the reservoir (Figures 13 and 14).

4.4.2. Relationship with Characteristic Parameters of Micropore Structure. The comparison results show that the correlation between the micropore throat characteristic parameters and the movable fluid saturation in the constant velocity mercury penetration experiment in the research area is better than that in the conventional mercury penetration experiment. Displacement pressure, maximum pore throat radius, average throat radius, sorting coefficient, and other parameters have a good correlation with movable fluid saturation (Figures 15–18). There is almost no correlation between the maximum mercury saturation parameter and the movable fluid saturation (Figure 19).

5. Conclusion

(1) The principle of conventional mercury penetration experiment is the same as that of constant-speed mercury penetration experiment. The theoretical model of the former experiment is a capillary tube bundle model with different radius. The maximum injection pressure is high and the experimental speed is fast. The experimental theoretical model of the latter is a pore throat capillary model with different radii. The experimental speed is very slow and it is almost a quasistatic process

(2) The physical property of C 7 reservoir is worse than that of C 6 reservoir, and the heterogeneity of reservoir pore throat is stronger. The pore structures of C 6 and C 7 are divided into four types, of which C 6 reservoir is of class I, II, and III micropore structures, and C 7 reservoir is of class III and IV micropore structures

(3) It can be seen from the example that the displacement pressure, total mercury saturation, and separation coefficient obtained by the constant rate mercury penetration experiment are smaller than those measured by the conventional mercury penetration experiment. The maximum throat radius and average throat radius obtained in the former experiment are larger than those obtained in the latter experiment

(4) The correlation between the micropore throat characteristic parameters and the movable fluid saturation in the constant velocity mercury penetration experiment in the research area is better than that in the conventional mercury penetration experiment

Data Availability

The experimental data used to support the findings of this study are included in the manuscript.

Conflicts of Interest

The author declares that there is no conflict of interest between the publication of this study and other scholars and monographs.

Acknowledgments

The authors would like to acknowledge the financial support from the Shaanxi Natural Science Basic Research Program, China (2022JQ-290).

References

[1] W. Li, Y. Zhang, F. Wang, J. Zhu, and B. Ye, "Application of constant-rate mercury penetration technique to study of pore throat characteristics of tight reservoir: a case study from the Upper Triassic Yanchang Formation in Ordos Basin," *Lithologic Reservoirs*, vol. 24, no. 6, pp. 60–65, 2012.

[2] X. Dianshi, S. Lu, Z. Lu, W. Huang, and M. Gu, "Combining nuclear magnetic resonance and rate-controlled porosimetry to probe the pore-throat structure of tight sandstones," *Petroleum Exploration and Development*, vol. 43, no. 6, pp. 1049–1059, 2016.

[3] Y. Jian, M. Jie, L. Jungang, C. Yan, F. Shengbin, and L. Weicheng, "Application of mercury injection and rate-controlled mercury penetration in quantitative characterization of microscopic pore structure of tight reservoirs: a case study of the Chang7 reservoir in Huachi-Heshui area, the Ordos Basin," *Petroleum Geology & Experiment*, vol. 37, no. 6, pp. 789–795, 2015.

[4] G. Hui, W. Meiqiang, and S. Shuilong, "Quantitative evaluation of micro-pore throat heterogeneity in extra-low permeability sandstone using constant rate mercury penetration-taking the Chang8 reservoir of Xifeng oilfield in Ordos Basin," *Progress in Geophysics*, vol. 28, no. 4, pp. 1900–1907, 2013.

[5] C. Lianxun, "Application of constant-rate intruding mercury and nuclear magnetic resonance method to low permeability reservoir evaluation," *Journal of Chengdu University of Technology (Science & Technology Edition)*, vol. 39, no. 4, pp. 430–433, 2012.

[6] G. Yongli and Z. Zhiguo, "Valuation on difference of pore throat structure of low permeability sandstone by constsp mercury penetration technique," *Geological Science and Technology Information*, vol. 30, no. 4, pp. 73–76, 2011.

[7] G. Hui, X. Wei, Y. Jianpeng, Z. Chuang, and S. Wei, "Pore throat characteristics of extra-ultra low permeability sandstone reservoir based on constant-rate mercury penetration technique," *Petroleum Geology & Experiment.*, vol. 33, no. 2, pp. 206–211, 2011.

[8] S. Tiaotiao, S. Wei, and H. Shengping, "Relationship between micro-pore structure and movable fluid saturation in low permeability reservoir," *Geological Science and Technology Information*, vol. 31, no. 4, pp. 81–85, 2012.

[9] Y. Shenglai and W. Junzhi, *Reservoir Physics*, Petroleum Industry Press, Beijing, 2004.

[10] V. Yakov and L. S. Win, "A practical approach to obtain primary drainage capillary pressure curves from NMR core and log data," *Petrophysics*, vol. 42, no. 4, pp. 334–343, 2001.

[11] M. H. Cohen and K. S. Mendelson, "Nuclear magnetic relaxation and the internal geometry of sedimentary rocks," *Journal of Applied Physics*, vol. 53, no. 2, pp. 1127–1135, 1982.

[12] W. Sun, Z. Qu, and G. Q. Tang, "Characterization of water injection in low-permeability rock using sandstone micromodels," *Journal of Petroleum Technology*, vol. 56, no. 5, pp. 71-72, 2004.

[13] W. Sun and G. Q. Tang, "Visual study of water injection in low permeable sandstone," *Journal of Canadian Petroleum Technology*, vol. 45, no. 11, pp. 21–26, 2006.

[14] Z. Hongbing, W. Furong, L. Jing, T. Tao, and S. Wu, "Characteristics of pore structure of intersalt shale oil reservoir by low-temperature nitrogen adsorption and high-pressure mercury pressure methods in Qianjiang Sag," *Bulletin of Geological Science and Technology*, vol. 40, no. 5, pp. 242–252, 2021.

[15] Y. Liu, X. Dong, Y. Lin, F. Chen, Y. Gao, and Z. Chen, "Quantitative characterization of pore structure of Lucaogou formation in Jimsar Sag," *Xinjiang Petroleum Geology*, vol. 40, no. 3, pp. 284–289, 2019.

[16] Z. Meng, S. Wei, D. Liu et al., "Combined mercury porosimetry to characterize the microscopic pore structure and pore size distribution of tight reservoirs: a case of Chang 6 reservoir in Wuqi area, Ordos Basin," *Geological Science and Technology Information*, vol. 38, no. 2, pp. 208–216, 2019.

[17] Z. Yang, Z. Ma, Q. Xiao, H. Guo, and Y. Luo, "Method for Al-sale prethroat measurements in tight reservoir cores and its application," *Journal of Southwest Petroleum University (Science & Technology Edition)*, vol. 40, no. 3, pp. 97–104, 2018.

[18] Q. Yan, Y. Zhang, H. Fu et al., "High pressure mercury injection and scanning electron microscopy applied to characterize micro- and nano-scale pore throats in tight sandstone reservoirs: a case study of the fourth member of Shahejie formation

in Yi176 block, Zhanhua Sag, Bohai Bay Basin," *Petroleum Geology & Experiment*, vol. 40, no. 2, pp. 280–287, 2018.

[19] X. Sun, X. Zhang, C. Lin, Z. Zhao, C. Ma, and J. Lin, "Quantitative E valuation method of HPMI pore throat distribution based on NMR calibration," *Rock and Mineral Analysis*, vol. 36, no. 6, pp. 601–607, 2017.

[20] N. R. Morrow, "Physics and thermodynamics of capillary action in porous media," *Industrial and Engineering Chemistry Research*, vol. 62, no. 6, pp. 32–56, 1970.

[21] S. He, C. Jiao, J. Wang, F. Luo, and L. Zou, "Discussion on the differences between constant-speed mercury injection and conventional mercury injection techniques," *Fault-Block Oil & Gas Field*, vol. 18, no. 2, pp. 235–237, 2011.

[22] P. Chen, S. Wang, D. Wang, X. Jia, and H. Qian, "Comparing the constant-speed mercury injection technique with the conventional mercury injection technique," *Xinjiang Geology*, vol. 31, no. S1, pp. 139–141, 2013.